Soc., **95**, 8650 (1973).
(12) R. Dallinger, unpublished result.
(13) E. R. Lippincott and R. D. Nelson, *Spectrochim. Acta*, **10**, 307 (1958).
(14) S. J. Cyvin, J. Brunvoll, and L. Schafer, *J. Chem. Phys.*, **54**, 1517 (1971).
(15) L. Hocks, J. Goffart, G. Duyckaerts and P. Teyssie, *Spectrochim. Acta, Part A*, **30**, 907 (1974).
(16) G. Herzberg, "Infrared and Raman Spectra", Van Nostrand, New York, N.Y. 1945, p 154.
(17) D. M. Duggan and D. N. Hendrickson, *Inorg. Chem.*, **14**, 955 (1975).
(18) T. G. Spiro and P. Stein, *Annu. Rev. Phys. Chem.*, **28**, 501 (1977).
(19) T. G. Spiro and P. Stein, *Indian J. Pure Appl. Phys.*, **16**, 213 (1978).
(20) The analysis is unaffected if the point group is D_{8d} (staggered rings) rather than D_{8h} (eclipsed rings).
(21) C. K. Jorgensen, "Absorption Spectra and Chemical Bonding in Complexes", Pergamon Press, New York, N.Y., 1962, pp 173–178.
(22) J. R. Nestor and T. G. Spiro, *J. Raman Spectrosc.*, **1**, 539 (1973).
(23) A. Avdeef, K. N. Raymond, K. O. Hodgson, and Z. Zalkin, *Inorg. Chem.*, **11**, 1083 (1972).
(24) F. Inagaki, M. Tasumi, and T. Miyazawa, *J. Mol. Spectrosc.*, **50**, 286 (1974).
(25) R. L. Mowery, Ph.D. Thesis, University of Virginia, 1976.
(26) In principle, the vibrational energies for the excited state at 466 cm^{-1} are not the same as those of the ground state, so that a frequency shift might be expected for the vibrational modes resonant under band III. The excited state must have essentially the same bonding as the ground state, however, as evidenced by the narrowness of the 466-cm^{-1} mode, and vibrational shifts are expected to be negligible.
(27) O. S. Mortensen, *Chem. Phys. Lett.*, **30**, 406 (1975).
(28) S. Sunder, R. Mendelsohn, and H. J. Bernstein, *J. Chem. Phys.*, **63**, 573 (1975).
(29) J. H. Van Vleck, "The Theory of Electric and Magnetic Susceptibilities", Oxford University Press, New York, N.Y., 1948.
(30) N. Edelstein, G. N. Lamar, F. Mares, and A. Streitwieser, Jr., *Chem. Phys. Lett.*, **8**, 399 (1971).
(31) J. Friedman and R. M. Hochstrasser, *Chem. Phys. Lett.*, **32**, 414 (1975).

Chemically Modified Electrodes. 13. Monolayer/Multilayer Coverage, Decay Kinetics, and Solvent and Interaction Effects for Ferrocenes Covalently Linked to Platinum Electrodes

Jerome R. Lenhard and Royce W. Murray*

Contribution from the Kenan Laboratories of Chemistry, University of North Carolina, Chapel Hill, North Carolina 27514. *Received June 23, 1978*

Abstract: Surface synthesis, electrochemical properties, and second-order ferricinium decay kinetics are described for a series of ferrocene carboxylic acids immobilized on PtO surfaces using alkylaminesilane chemistry. For immobilized ferrocenylphenylacetamide, surface activity nonideality parameters are smaller and ferricinium stability is enhanced for immobilized multilayers as compared to monolayers.

The reactions which an electrode-immobilized molecular charge-transfer state can undergo during repetitive cycling between different oxidation states are pertinent to any eventual electrocatalytic utility. Appreciation of the various chemical stabilizing and destabilizing factors in the surface molecular structures is presently fragmentary. Efforts[1-6] have been both limited and hampered by modest chemical lifetimes of available surface structures plus poor definition (signal/background) of electrochemical electron-transfer responses. This paper describes the synthesis and properties of a series of ferrocenecarboxylic acids demonstrably covalently linked to electrogenerated Pt|PtO surfaces using the alkylaminesilane 3-(2-aminoethylamino)propyltrimethoxysilane (*en*-silane) and carbodiimide-assisted amidization (reaction 1). Ferrocenylphenylacetic acid, I, immobilized in this manner, exhibits remarkable chemical and electrochemical stability and well-defined cyclic voltammetric response. We present here quantitative information on decay kinetics of redox molecules immobilized on electrodes. The decay, interestingly, is second order in ferricinium. We also describe an analysis of interactions based on solvent and surface activity effects. We have prepared both monolayer and multilayer coverages of I on electrodes and report the first comparison of electrochemistry, chemical stability, and surface activity of a covalently linked molecule at monolayer and multilayer coverage.

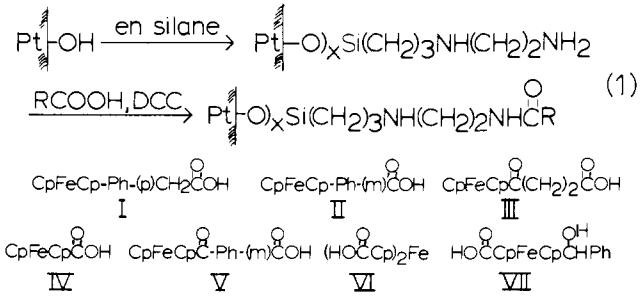

Experimental Section

Chemicals. 3-(2-Aminoethylamino)propyltrimethoxysilane (*en*-silane, PCR) was distilled when received and routinely redistilled thereafter. Acetonitrile (Spectrograde, MCB) was dried over molecular sieves and benzene over sodium. Dicyclohexylcarbodiimide (DCC, Aldrich) was used as received. Tetraethylammonium perchlorate (Eastman, recrystallized three times from water) was supporting electrolyte throughout.

All ferrocene compounds were courtesy of Professor W. F. Little (UNC, Chapel Hill) except IV and VI (Aldrich) and 1,1′-bis(trimethylsilyl)ferricinium tetrafluoroborate (from Professor M. Wrighton, MIT).

Apparatus. Current-potential waves were observed by cyclic voltammetry using electrochemical equipment and cells of conventional design. Potentials are referenced to a NaCl saturated calomel electrode (SSCE). Fast sweep data were obtained with a PARC Model 173 potentiostat and *iR* compensation. Pt disk electrodes (area 0.102 to 0.153 cm^2) were silver soldered to brass rods; some for interchangeable use in electron spectroscopy and electrochemical experiments were fitted with Teflon shrouds. X-ray (Mg anode) photoelectron spectra (XPES) were obtained with a DuPont 650B electron spectrometer,[7] data acquisition and manipulation on which were facilitated by a microprocessor system.[8] Intensities are expressed as integrated peak areas.

Procedure. Mirror polished (1 micron diamond paste) Pt disk electrodes are cleaned by 5-min anodization in 1 M H_2SO_4 (+1.9 V

0002-7863/78/1500-7870$01.00/0

Table I. XPES of Ferrocenes and PtO|*en*|1 Electrodes

compd	binding energies,[a] eV	$I_{Fe,2p_{3/2}}/I_{Si,2s}$	$I_{Fe,2p_{3/2}}/I_{N,1s}$
$[(CH_3)_3SiCp]_2Fe^+BF_4^-$	709.5[b]	9.06[c]	
Cp_2Fe	707.5		
$CH_3CONHPhCpFeCp$	708.2		5.26[d,e]
$EtOOCCH_2PhCpFeCp$[f]	708.1		
PtO/*en*/$COCH_2PhCpFeCp$[g]	708.0 ± 0.1[h]	3.10 ± 1.28[h]	1.50 ± 0.58[h,i]

	Intensity Results for PtO|*en*|1 Electrodes atom ratios[j]			
electrode[l]	Fe/Si	2(Fe/N)[k]	N/Si	$I_{Fe,2p_{3/2}}/I_{Pt_{5/2,7/2}}$[n]
highest coupling, % ($\Gamma_{corr} = 1.7 \times 10^{-10}$ mol/cm^2)	0.87	1.05	1.67[m]	0.049
lowest coupling, % ($\Gamma_{corr} = 1.9 \times 10^{-10}$ mol/cm^2)	0.19	0.22	1.70[m]	0.014
average[h]	0.35 ± 0.14	0.50 ± 0.19	1.46 ± 0.61	0.031

[a] Referenced to C 1s as 285.0 eV. [b] Ferricinium sample. [c] Theoretical sensitivity ratio is $(10.5/0.855)(546/1101)^{0.75} = 7.26$, in fair agreement with this standard. [d] Theoretical sensitivity ratio is $(10.5/1.78)(546/854)^{0.75} = 4.22$, in fair agreement with this standard. [e] The ratio 9.06/5.26 = 1.72 = N/Si 2s sensitivity agrees with a previous estimate.[6] [f] Analogue of immobilized 1. [g] PtO|*en*|1 electrode. [h] Average of data from seven electrodes. [i] N 1s corrected for minor background peak[6] observed on PtO. [j] Calculated using experimental sensitivity ratios above. [k] Factor of 2 accounts for two nitrogens in *en*-silane. [l] "Highest and lowest" are extremes measured. [m] Similar to N/Si previously measured on *en*-silanized metal oxide electrodes.[6] [n] In qualitative terms this ratio correlates with the Fe/Si reaction yield data, the ratios increasing or decreasing together. Fluctuations in amidization reaction yield, plus possible variation in silane coverage, preclude meaningful quantitative correlation between I_{Fe}/I_{Pt} and electrochemically measured ferrocene coverage of the sort established in another ferrocene electrode study.[13]

vs. SCE) followed by potential cycling between hydrogen and oxygen discharge waves until the characteristic clean Pt wave pattern is obtained.[9] Microscopic area was determined by integration of the hydrogen absorption waves.[10] The electrode is oxidized at +1.1 V until current decays to a small value, washed with distilled water, vacuum-oven dried (15 minutes, 50°C), and suspended (avoiding contact with the brass backing) in a stirred anhydrous ca. 5% *en*-silane solution in benzene, under N_2, for 5 min at room temperature. The silanized surface is copiously rinsed three times (under N_2) with benzene and then sequentially with CH_3CN and CH_3OH. This electrode surface, designated PtO|*en*, is amidized by exposure to a mixture of the ferrocenecarboxylic acid and excess DCC in CH_3CN for 20 h. Subsequent rinsing with CH_3CN for 24 h preceeds electrochemical or ESCA experiments.

In contrast to experiments with a different silane,[2] no particular differences in silanization results were noted if the Pt electrode was oxidized at +1.9 V or in concentrated HNO_3. Perhaps some phase of the reaction protocol levels the Pt surface oxidation condition to a common state.

Adsorption Controls. To demonstrate that adsorption does not masquerade for reaction 1, key ingredients (e.g., silane, carboxylic acid group) were serially omitted in control reactions. A PtO surface treated with DCC plus ferrocene I exhibits no significant ferrocene cyclic voltammetry (coverage ca. 0.2×10^{-10} mol/cm^2) or Fe $2p_{3/2}$ XPES response. Similarly, no ferrocene electrochemistry results from exposing a PtO|*en* surface to a CH_3CN solution of DCC and biphenylferrocene under amidization reaction conditions. Control experiments were likewise carried out for the other ferrocenes, except V and VII, and (negative) results support reaction 1 amide bond formation as for 1.

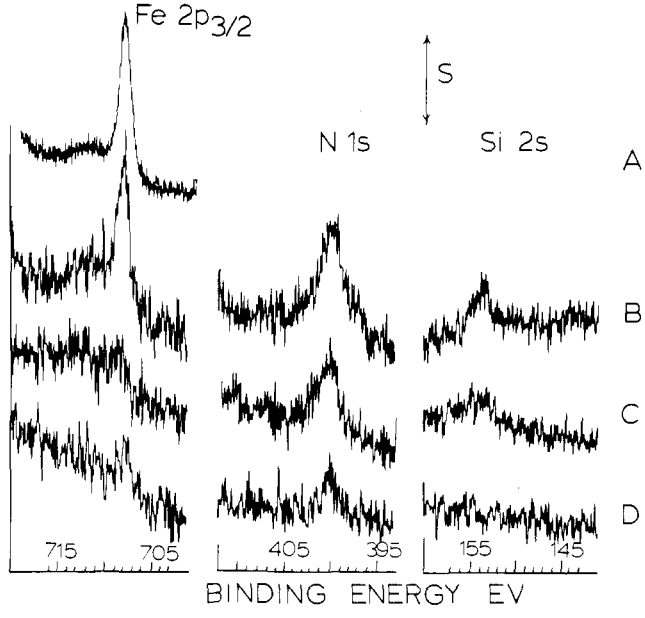

Figure 1. XPES spectra of chemically modified PtO electrodes. Curve A, pure 4-(ferrocenyl)phenylacetate (powder); curve B, PtO|*en*|1; curve C, PtO|*en*|1 after potentiostating at 0.7 V vs. SSCE until ferrocene wave disappears; curve D, PtO control treated with DCC plus 1 for 20 h; S = 1528 counts (A, B, C), 769 counts (D).

Results and Discussion

Immobilized 4-(Ferrocenyl)phenylacetamide. Fe $2p_{3/2}$, N 1s, and Si 2s XPES bands on PtO|*en* electrodes amidized (reaction 1) with 4-(ferrocenyl)phenylacetic acid (I) are shown in Figure 1, as is Fe $2p_{3/2}$ for pure ethyl 4-(ferrocenyl)phenylacetate. The ferrocene ester Fe $2p_{3/2}$ binding energy (Table I) (708.1 eV) and that observed on the PtO|*en*|1 electrodes (708.0 eV) are in excellent agreement. PtO|*en*|1 electrodes in 0.1 M $Et_4N^+ClO_4^-/CH_3CN$ give symmetrical, well-defined, cyclic voltammograms as illustrated by curve A of Figure 2. Data are given in Table II, entries A and B. Peak currents are accurately proportional to potential scan rate (0.02–20 V/s) and peak potential separations (ΔE_p) are small and scan-rate independent.[11] The formal potential ($E°'$) for the surface wave of Figure 2 is 0.442 V vs. SSCE and is 0.437 ± 0.020 V for the 25 PtO|*en*|1 electrodes examined. $E°'$ for the solution analogue ethyl 4-(ferrocenyl)phenylacetate is a very similar 0.427 V. Extensive (days to weeks) soaking in nonaqueous solvents has little or no degrading effect on subsequent electrochemistry or Fe, N, and Si XPES. Both XPES and electrochemical tests for interfering adsorption effects were negative (see Experimental Section).[15]

Thus, XPES and electrochemical data fully support stable immobilization of ferrocene I via amide bond formation as purported in reaction 1. The voltammetric wave observed in Figure 2, curve A, can be ascribed to the one-electron oxidation-reduction of I as a surface ferrocene $\rightleftharpoons$ ferricinium charge-transfer state.

The reaction yield of the amidization step in reaction 1 as deduced from Fe/Si and Fe/N XPES intensity ratios on

Table II. Electrochemical Results for Ferrocenes Immobilized on Pt Electrodes, in $Et_4N^+ClO_4^-/CH_3CN$

entry	electrode	no. of samples	$E^{\circ\prime}$ soln,[a] V vs. SSCE	$E^{\circ\prime}$ surf,[b] V vs. SSCE	ΔE_p, mV	E_{fwhm},[c] mV	$\Gamma_{corr} \times 10^{10}$ mol/cm^2 [d]
A	PtO|*en*|I monolayer results[e]	13	0.427	0.437 ± 0.020	22 ± 10	146 ± 20	1.25 to 3.30 (av 1.89)
B	kinetic study	(0.5 h)[f]		0.438	27	160	0.39
		(1.25 h)		0.432	27	160	0.44
		(2.2 h)		0.430	24	151	0.71
		(4.0 h)		0.437	21	152	0.74
		(8.0 h)		0.434	26	148	1.10
		(20 h)		0.431	32	155	1.28
		(28 h)		0.421	22	168	0.96
C	larger coverages[e]						
	series A	1		0.461	28	130	4.3
		1		0.450	30	130	3.9
		1		0.436	20	116	4.2
	series B	1		0.441	21	98	7.1
	series C	1		0.442	22	99	8.2
D	PtO|*en*|II	5	0.470	0.448	17		av 0.51
E	PtO|*en*|III	6	0.633	0.613	28		av 0.77
F	PtO|*en*|IV	3	0.628	0.588	60		av 0.47
G	PtO|*en*|V	2	0.661	0.658	37		av 0.18
H	PtO|*en*|VI	3	0.838	0.757	122		av 0.32
I	PtO|*en*|VII	2	0.636	0.592	27		av 0.18

[a] The solution analogues are the corresponding carboxylic acids; $E^{\circ\prime}_{soln}$ agrees to ca. 5 mV with previous values,[17d,e] except for VI. [b] $E^{\circ\prime}_{surf} = (E_{p,c} + E_{p,a})/2$. [c] Width of cyclic voltammetric wave at half peak current maximum. [d] Γ_{corr} determined after cycling 10–20 times to reduce background current, from cyclic voltammogram charge divided by 1.7 roughness factor. [e] See text. [f] Amidization reaction time study. All others prepared using 20 h amide-coupling time.

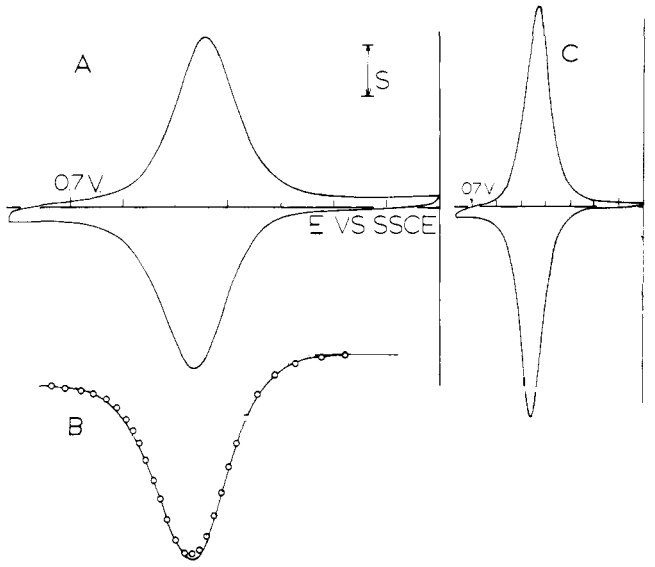

Figure 2. Cyclic voltammograms at PtO|*en*|I electrodes in 0.1 M Et_4NClO_4/CH_3CN. Curve A, monolayer example (Table II), S = 14 ua/cm^2, 200 mv/s; curve B, comparison of experimental (−) and theoretical (○) cyclic voltammograms, 100 mV/s; curve C, multilayer example (Table II, series B), S = 30.2 ua/cm^2, 200 mV/s. S corrected for surface roughness.

PtO|*en*|I surfaces is given in Table I. The high, low, and average surface atom ratios show that the surface reaction involves on the average about 50% of the primary amine sites on PtO|*en* but yields for specific electrodes can be much higher (90%), and lower (20%). Observed N/Si atom ratios were normal.

The surface coverage (Γ_{corr}) of immobilized ferrocene I is evaluated from the charge under the current-potential wave (Figure 2) with correction for electrode roughness.[14] Γ_{corr} on most (75%) PtO|*en*|I electrodes is between 1.25 and 3.3 × 10^{-10} mol/cm^2 (entry A, Table II). Molecular models of immobilized I give compatible numbers; Γ_{corr} = 3.3 × 10^{-10} mol/cm^2 for a rather loose packing with connecting chain extended perpendicular from the electrode surface, and 1.2 × 10^{-10} mol/cm^2 for a high proportion of "lying-flat" or cyclized[6] chains. These results indicate that the PtO|*en*|I electrode bears an approximate monomolecular layer of immobilized I. Some larger electrode coverages (entry C) are discussed later.

Entry B of Table II gives data for PtO|*en*|I electrodes for different DCC assisted amidization reaction times. Fe $2p_{3/2}$ XPES intensities parallel the time change in surface coverage. Only Γ_{corr} varies regularly with time; $E^{\circ\prime}$ and ΔE_p do not systematically[5] change. The latter observation is significant in that it compares a rate sensitive parameter[11] (e.g., ΔE_p) to coverage on an organosilane-based modified electrode where a saturated molecular chain separates electrode and electroactive moiety. The result (e.g., no effect) concurs with the "floppy model" view[1,6] of the electron-transfer event.

PtO|*en*|I electrodes are chemically and electrochemically stable. Continuous cycling between oxidized and reduced immobilized ferrocene I causes only slow decay of the cyclic voltammetric waves as illustrated by the 26-h cycling experiment of Figure 3. Exhaustive (>95%) depletion of electroactive I typically occurs after ca. 15 000 scans, but electrodes with significantly longer (3×) lifetimes have been prepared. This stability is comparable to that of an immobilized ferrocene prepared by Wrighton and co-workers.[16]

Figure 1, curve C, shows XPES of a PtO|*en*|I electrode decomposed by potentiostating at +0.7 V until a cyclic voltammogram exhibits no ferrocene wave. The concurrent loss of ferrocene electrochemistry and XPES Fe $2p_{3/2}$ implies that all surface bound ferrocene is electroactive. Persistence of the N 1s and Si 2s XPES bands in curve C suggests that the Pt-alkylaminesilane linkage remains intact, decomposition proceeding through rupture of amide bond or metal sandwich. Since exacting comparisons between curves B and C of Figure 1 are difficult, however, we are reluctant to claim quantitative stability for the Pt-alkylaminesilane surface linkage.

Table III. Decay Kinetics[a] for Immobilized Ferricinium

electrode	$\Gamma_{corr}(t = 0)$, mol/cm²	$t^{1/2}$, min[b]	k_{obsd}, cm²/(mol s)[c] hold	k_{obsd}, cm²/(mol s)[c] cycle
PtO|*en*|I	1.25×10^{-10}	100	9.3×10^5	(1.6×10^6)[d]
	1.47×10^{-10}	360	2.3×10^5	(3.8×10^5)[d]
	3.01×10^{-10}	180		3.0×10^5
	2.16×10^{-10}	185	3.8×10^5	(6.3×10^5)[d]
	1.25×10^{-10}	170		7.3×10^5
	4.12×10^{-10}	750		5.3×10^4 (multilayer)
PtO|*en*|III	2.74×10^{-10}	51		1.2×10^7[e]
	1.54×10^{-10}	26		4.2×10^6
PtO|*en*|II	0.23×10^{-10}	145		5.7×10^6
	0.43×10^{-10}	180		2.2×10^6
	0.29×10^{-10}	105		5.4×10^6
PtO|*en*|VI	0.35×10^{-10}	~8		6.0×10^7[e]
	0.71×10^{-10}	~10		2.4×10^7[e]
PtO|*en*|V	0.41×10^{-10}	~11		3.7×10^7[e]

[a] Sample decomposition prompted by potential cycling from 0 to 0.7 V vs. SSCE (cycle) or potentiostating at 0.7 V (hold). [b] Time at which $\Gamma = \Gamma(t = 0)/2$. [c] Slope of $1/\Gamma_{corr}$ vs. time plot. [d] Numbers in parentheses are "hold" time axis converted to equivalent "cycle" time by dividing by 0.6, the fraction of a cycle spent in the ferricinium state. [e] k_{obsd} calculated from $[t^{1/2}\Gamma_{corr}(t = 0)]^{-1}$.

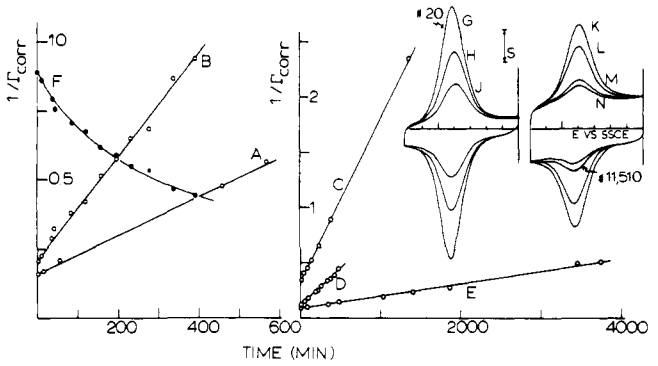

Figure 3. Second-order decay kinetic plots for PtO|*en*|I electrodes continuously cycled (0 to 0.7 V vs. SSCE, curves C, D, and E) or held at 0.7 V (curves A and B). Curve F is the first-order decay plot for data of curve B. Curves G, H, and J are PtO|*en*|I electrode cyclic voltammograms showing 20th, 990th, and 3042nd successive scans, respectively, $S = 9.5$ ua/cm². Curves K–N show the 4246th, 6620th, 11510th, and 13622nd successive scans, $S = 2.9$ ua/cm², 200 mV/s.

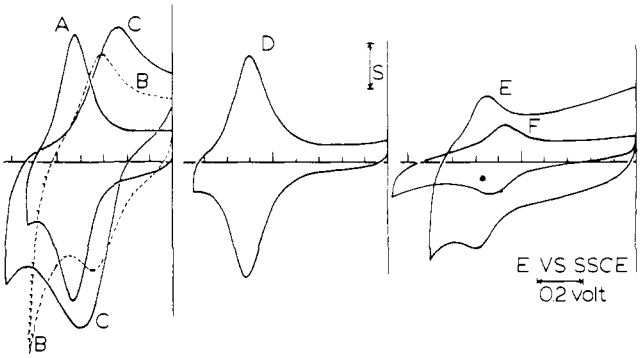

Figure 4. Cyclic voltammograms: 200 mV/s, 0.1 M Et_4NClO_4. Curve A, PtO|*en*|I in CH_3CN, $S = 4.9$ ua/cm²; curve B, PtO|*en*|I in 9:1 H_2O/CH_3CN, $S = 6.5$ ua/cm²; curve C, PtO|*en*|I in H_2O (1 M KCl electrolyte, pH 4), $S = 19.4$ ua/cm²; curve D, PtO|*en*|III in CH_3CN, $S = 8.7$ ua/cm² (PtO|*en*|II gives a similar response); curve E, PtO|*en*|V in CH_3CN, $S = 5.6$ ua/cm² (PtO|*en*|VI and PtO|*en*|VII are similar); curve F, PtO|*en*|IV in CH_3CN, $S = 13.4$ ua/cm²; S is roughness corrected.

The PtO|*en*|I electrode is in general a well-mannered, routinely preparable, immobilized charge-transfer surface state. Its stability and cleanly defined electrochemistry permit quantitative accessory studies of decay kinetics, surface activity, and multilayer forms as described in following sections.

Other Immobilized Ferrocenes. The other ferrocene carboxylic acids II–VII can be immobilized on PtO|*en* surfaces as illustrated by Figure 4 (curves D–F) and data in Table II. Immediately obvious is that ΔE_p, Γ_{corr}, and definition of the surface electrochemistry are quite variable. Formal potentials for all, however, are similar to those of solution analogues (Table II), e.g., they are governed by substituent effects[17] in the same manner as the solution ferrocenes, over a ca. 300-mV range. Stability of the immobilized ferrocenes toward repetitive charge state cycling is also substituent dependent as discussed in the next section.

Decay Kinetics of Ferrocene Electrodes. No detailed stability analysis for a chemically modified electrode has yet been presented. Pertinent questions include any distinction between turnover and static stability of the different oxidation states, and the relation of decay kinetics to surface molecular structure. The immobilized ferrocenes proved well suited to exploring these questions.

When PtO|*en*|I electrodes are cycled between ferrocene and ferricinium states, or statically potentiostated at +0.70 V, a slow decay in cyclic voltammetric response occurs as in Figure 3. No decay occurs upon storage (days to weeks) under CH_3CN[18] or for potentiostating (24 h) at 0 V (ferrocene state). Ferricinium is the less stable state, as expected. Decay kinetics can be analyzed by monitoring the active charge state population (e.g., Γ_{corr}) as a function of potential cycling or potentiostating time. Plots of kinetic data according to first-order decay are uniformly nonlinear (for PtO|*en*|I and other ferrocenes); see the typical curve F of Figure 3. The decay of immobilized ferrocene is not first order.

Second-order plots for PtO|*en*|I electrodes, shown in Figure 3, are typically linear over at least 3 half-lives (e.g., to $\Gamma = 0.12\ \Gamma_{init}$). Apparent second-order rate constants k^{obsd} taken from the slopes of the potentiostated (curves A and B) and cycling (curves C–E) decay plots are given in Table III. Upon conversion of potentiostated experimental time to equivalent potential cycling time, k^{obsd} values for the two decay modes are in satisfactory agreement. With the exception of the multilayer electrode (vide infra), k^{obsd} does not appear to depend on the initial surface concentration. Thus, decay of the layer of charge-transfer states depends on time spent as ferricinium (static stability) not on events attendant to electron transfer (turnover stability), and the decay rate is second order in ferricinium.

It is well known[19a,b] that ferricinium decay is first order in aqueous medium. The only nonaqueous data[20] available

suggest second-order kinetics in CH_3CN, but are not unequivocal.

Second-order decay of immobilized ferrocene 1 appears to be without clear precedent.

XPES data show that decay occurs by loss of surface iron with apparent retention of alkylaminesilane. It is difficult to imagine how a process involving two *immobilized* ferriciniums could persist to long times when the surface has become "dilute". The reaction may well include an intermediate diffusion step. On the other hand, the average ferricinium site-site distance when $\Gamma_{corr} = 0.16 \times 10^{-10}$ mol/cm^2 (third $t^{1/2}$ for curve C, Figure 3) is ~18 Å as compared to the ~22 Å length of the (noncyclized) immobilized *en*-silane-1 structure. On this basis immobilized "neighbor collisions" remain possible at this dilute coverage level. Also, the effective neighbor collision frequency at this or higher coverages is probably large compared to solution collision rates at ordinary concentrations, possibly bringing into play pathways of chemical reactivity unimportant in solution. Further speculation on this second-order rate control does not seem worthwhile without additional information.

Electodes prepared using the other ferrocenes also exhibit linear $1/\Gamma_{corr}$ vs. time decay plots and apparent second-order kinetics. Results (Table III) are less accurate for electrodes with low Γ_{corr}, but stability differences are obvious. The reactivity order, I < II ≈ III < V ≈ VI, is precisely that expected on the basis of ferricinium destabilization by electron-withdrawing substituents, as observed in solution studies.[19b,20] These results document a parallel between surface and solution order of reactivity.

Multilayer Coverages on PtO|*en*|I Electrodes. In the course of immobilizing ferrocenes and other reagents on Pt electrodes with organosilane reagents, we occasionally produce samples with (roughness corrected) coverage of electroactive species 2–50 times too large to be reconciled with monomolecular layers. Silane polymer present in the reagent or formed during reaction with the PtO surface becomes bound to the electrode in a manner leaving the amine or other silane functionality in a reactive state. Polymerization of the silane is induced by traces of adventitious or deliberate moisture. Amidization of these surfaces has led to immobilization of several redox couples exhibiting well-defined, stable electrochemistry and Γ extending to 9.6×10^{-9} mol/cm^2. Reproducible fabrication of these interesting multilayer charge-transfer surfaces is difficult, yet we have prepared a sufficient number to warrant discussion. In particular, multilayer immobilization of 1 offers an opportunity for a monolayer/multilayer comparison.

Table II gives data (entry C) for three PtO|*en*|I electrode series yielding coverage larger than the model-estimated monolayer 3.3×10^{-10} mol/cm^2. These electrodes exhibit nearly ideal[12] cyclic voltammetric behavior (Figure 2, curve C) including small ΔE_p, wave symmetry and narrow width, low relative background current, and extreme stability to repetitive cycling. Peak current is linearly dependent on sweep rate, while ΔE_p and wave shape are independent of sweep rate from 0.1 to 20 V/s. $E^{\circ\prime}$ and ΔE_p values are indistinguishable from monolayer coverage electrodes, but interestingly, the multilayer wave at highest coverage is significantly sharper than on monolayer PtO|*en*|I electrodes and other previously reported ferrocene polymer electrodes.[16,21]

The narrow peak widths approach the 91 mV value predicted[12,22] for zero stabilizing or destabilizing neighbor-neighbor interactions as discussed below. The ferrocene sites on these multilayer electrodes experience diminished ferrocene/ferrocene/ferricinium interactions, implying that the *higher* surface coverage actually yields a more *dilute* structure than for the monolayer examples. We speculate that on these surfaces oligomerization has produced a flexible chain structure propagating two dimensionally from the electrode surface with little or no cross-linking.

Like monolayer PtO|*en*|I electrodes, the multilayer versions are little affected by extensive rinsing with solvents. Extreme stability toward repetitive potential cycling is another characteristic. Decay is again second order (Figure 3) but the decay constant is ca. 10× smaller (Table III). Some PtO|*en*|1 multilayer electrodes require ca. 50 000 cycles, for >90% depletion. The enhanced stability toward second-order decay is consistent with a surface structure diluted in comparison to the monolayer variety. Like the monolayer electrodes, decay is accomplished by a gradual cathodic shift of $E^{\circ\prime}$.

Obviously the properties of these multilayer electrodes pose interesting extensions of the fundamental questions applicable to the monolayer surfaces.

Shape of Current–Potential Waves for PtO|*en*|I Electrodes. The shape and width of current–potential peaks for immobilized molecular charge-transfer states are sensitive to interactions with their microenvironment. Brown and Anson,[5] following Laviron,[22] cast this sensitivity in terms of surface activities exponentially dependent on interaction parameters, r_O and r_R, for adsorbed oxidized and reduced states, respectively. In the theory, $E^{\circ\prime} \neq f(\Gamma)$ when $r_O = r_R = r$, $r \neq f(\Gamma)$, and negative r corresponds to destabilizing or repulsive interactions among oxidized and reduced states and broadened current–potential waves. Thus far, all reported cyclic voltammetric waves for immobilized charge-transfer states are substantially broader ($E_{fwhm} > 91$ mV) than expected[12,22] for the zero interaction situation.

Current–potential patterns for PtO|*en*|I electrodes were compared to the surface activity theory[5] using a least-squares computation and a cubic equation base line contour.[23] The fit to anodic (Figure 2) and cathodic peaks is reasonable and comparable to that for adsorbed materials.[5] Since $E^{\circ\prime}_{surf}$ (±4 mV) $\neq f(\Gamma_{corr})$ (entry B, Table II), r_O and r_R were equated. Minor (but systematic) mismatch appears near the current peak and trailing edge. Results for r, which is negative, appear in Table IV.

Although the current–potential wave shape for an individual selected electrode is consistent with the surface activity theory,[5] the theory does not anticipate such features as the systematic change of r with Γ (Table IV) or the constant $r\Gamma$ product (e.g., constant E_{fwhm}[22,23]) observed for monolayer PtO|*en*|I electrodes (Table II). The origin of these features remains unclear.

The relationship of r to Γ on electrodes undergoing decay (in repetitive cycling experiments) differs from that of electrodes with synthesized coverage levels (entry B, Table II) in that $E^{\circ\prime}$ for the decaying ferrocene shifts with coverage. The difference may be that during decay, Γ_{corr} is not simply diluted, but the ferrocene site microenvironment gradually becomes an array of decay sites which are (interactively) distinct from free *en* sites. Inclusion of a third parameter[23] in the theory for ferrocene and ferricinium site interaction with decay sites (at population $\Gamma_{corr}(t = 0) - \Gamma_{corr}(t)$) predicts a linear variation of $E^{\circ\prime}$ with $\Gamma_{corr}(t)$, which is in fact observed (Figure 5). This result indicates that, if the formalism of surface activity is used to represent current–potential patterns,[5] interaction effects with all neighbor sites, not just other charge-transfer states, can be important.

PtO|*en*|I Electrodes in Aqueous Media. Solvent effects on electron transfers of electrode-immobilized charge-transfer states provide another probe into their interfacial microenvironment. We thought it of interest to examine electrochemistry at PtO|*en*|1 electrodes in aqueous media, where unattached 1 and its ester are insoluble.

Gradual addition of H_2O to 0.1 M $Et_4N^+ClO_4^-/CH_3CN$ contacting a PtO|*en*|1 electrode reveals a continuing cathodic shift[24] in $E^{\circ\prime}$ and a small one-time change in ΔE_p (Figure 4, curves A and B). In an entirely aqueous medium, 1 M KCl/

Table IV. Interaction Parameters for PtO|*en*|I Electrodes

sample	$\Gamma \times 10^{10}$, mol cm^{-2}	$r \times 10^{-9}$, cm^2 mol^{-1}
1	2.5	−4.1
2	2.5	−3.0
3	3.3	−2.4
4	4.2	−1.1
5	6.7	−0.3

H_2O (pH 4), $E^{\circ\prime}$ is further shifted but ΔE_p is abruptly much larger (curve C).

The effects on ΔE_p are interesting and are being further explored. The results suggest a slowed charge transfer in KCl/H_2O associated with poor solvation of I and/or of the organic layer at the electrode-water interface. That a small proportion of CH_3CN in the H_2O yields much the same ΔE_p as the reverse situation means CH_3CN may preferentially solvate the organic interface.

The PtO|*en*|I electrode is stable toward soaking in water but when cycled to the ferricinium state undergoes ca. 90% decay in 2000 potential cycles.

Amine Chemisorption on Pt. In an experiment exploring the possible role of alkylamine in bonding of alkylaminesilane to Pt, we find that exposure of oxidized Pt electrodes to benzene solutions of butylamine and *N*-ethylethylenediamine (models of the silane-alkylamine functionality) followed by "amide coupling" to I produces no immobilized ferrocene electrochemistry, affirming our belief that PtOSi bonding dominates in the attachment of alkylaminesilanes to Pt electrodes.

However, exposure of oxidized Pt electrodes to benzene solutions of amines bearing at least two primary sites (e.g., ethylenediamine or tetraethylenepentamine) followed by washing and amide coupling (using I) does yield stable surface-immobilized ferrocene waves at small coverage levels. This strong chemisorption underscores the importance of regular *en*-silane purification as practiced throughout this report.

Discussion

The favorable properties of immobilized ferrocene charge-transfer states described here permit an investigation of stabilizing and destabilizing factors in electrode-immobilized surface structures more detailed than heretofore presented. The formal potential $E^{\circ\prime}$ and ferricinium chemical reactivities of the immobilized ferrocenes are ordered as anticipated from their solution counterparts; in this sense the modified Pt electrode's lifetime is associated with that of the chosen ferrocene.

Additional features emerge, however. Decay of immobilized I follows a second-order rate law as compared to first order (in aqueous solution). The high reaction order (if a diffusing step is not involved) means that the PtO|*en*|I surface does not exhibit features of site isolation, or hyperentropy,[25] in either its monolayer (two dimensional) or multilayer (three dimensional) forms. Second, immobilization of the same ferrocene I in both monolayer and multilayer forms revealed similar properties in all respects except greatly diminished interaction effects and decay rate for the multilayer version. These differences justify our otherwise somewhat arbitrary coverage-model comparison and subsequent separation of samples into monolayer and multilayer forms based on coverage >3.3 × 10^{-10} mol/cm^2. The enhanced stability of multilayer PtO|*en*|I shows that the manner of binding can play as important a role in chemical reactivity as that intrinsic to the ferricinium itself.

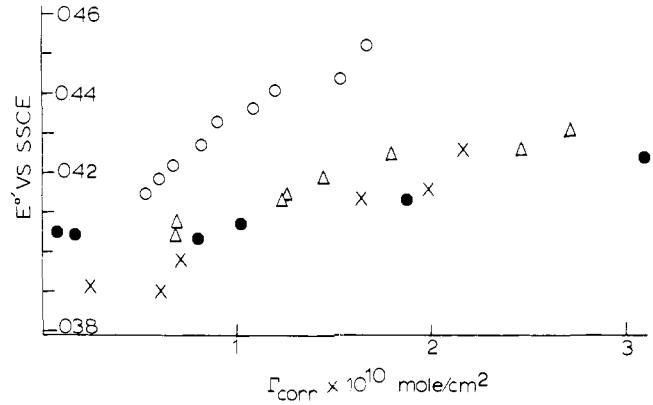

Figure 5. Plots of $E^{\circ\prime}$ vs. Γ_{corr} for several PtO|*en*|I electrodes subjected to extensive cycling or holding at 0.7 V.

Finally, quantitative characterization of stabilizing and destabilizing surface chemistry as attempted here is important in distinguishing the merits of different chemical strategies evolved for immobilizing the same or related charge-transfer states.

Acknowledgment. This research was supported by a grant from the National Science Foundation. The authors acknowledge with gratitude generous gifts of ferrocene derivatives from Professor W. F. Little, assistance with XPES spectra from M. Umana, and assistance with surface activity calculations from D. F. Smith.

References and Notes

(1) P. R. Moses and R. W. Murray, *J. Am. Chem. Soc.*, **98**, 7435 (1976).
(2) J. R. Lenhard and R. W. Murray, *J. Electroanal. Chem.*, **78**, 195 (1977).
(3) A. Diaz, *J. Am. Chem. Soc.*, **99**, 5838 (1977).
(4) J. C. Lennox and R. W. Murray, *J. Am. Chem. Soc.*, **100**, 3710 (1978).
(5) A. P. Brown and F. C. Anson, *Anal. Chem.*, **49**, 1589 (1977).
(6) P. R. Moses, L. M. Wier, J. C. Lennox, H. O. Finklea, J. R. Lenhard, and R. W. Murray, *Anal. Chem.*, **50**, 576 (1978).
(7) P. R. Moses, L. Wier, and R. W. Murray, *Anal. Chem.*, **47**, 1882 (1975).
(8) C. N. Reilley and W. S. Woodward, to be published.
(9) H. Angerstein-Kozlowska, B. E. Conway, and W. B. A. Sharp, Jr., *J. Electroanal. Chem.*, **43**, 9 (1973).
(10) T. Biegler, D. A. J. Rand, and R. Woods, *J. Electroanal. Chem.*, **29**, 269 (1971).
(11) $\Delta E_p = 0$ for fast electron exchange[12] and increases with scan rate for slow exchange. The lack of scan rate dependence of ΔE_p on PtO|*en*|I electrodes indicates that change-transfer kinetics are not responsible for the observed ΔE_p.
(12) R. F. Lane and A. T. Hubbard, *J. Phys. Chem.*, **77**, 1401 (1973).
(13) A. Fischer, M. Wrighton, M. Umana, and R. W. Murray, unpublished results, 1978.
(14) Γ on chemically modified electrodes reported so far are uncorrected for microscopic roughness. Our roughness correction, based on hydrogen adsorption on Pt, is probably an upper limit.
(15) Contact of PtO|en with I in the absence of DCC results in some ($\Gamma = 0.7 \times 10^{-10}$ mol/cm^2) unassisted surface amide coupling. Stability and electrochemical properties are similar to typical PtO|*en*|I electrodes.
(16) M. S. Wrighton, R. G. Austin, A. B. Bocarsly, J. M. Bolts, O. Haas, K. D. Legg, L. Nadjo, and M. Palazzotto, *J. Electroanal. Chem.*, **87**, 429 (1978).
(17) (a) H. Hennig and O. Gurtler, *Organometal. Chem.*, **11**, 307 (1967); (b) J. G. Mason and N. Rosenblum, *J. Am. Chem. Soc.*, **82**, 4208 (1960); (c) T. Kuwana, D. E. Bublitz, and G. Hoh, *ibid.*, **82**, 5811 (1960); (d) W. F. Little, C. N. Reilley, J. D. Johnson, K. N. Lynn, and A. P. Sanders, *ibid.*, **86**, 1376 (1964); (e) W. F. Little, C. N. Reilley, J. D. Johnson, and A. P. Sanders, *ibid.*, **86**, 1382 (1964).
(18) The other ferrocene surfaces are similarly storable. Air-dry storage often leads to large ΔE_p.
(19) (a) A. A. Pendin, M. S. Zakhar'evskii, and P. K. Leont'evskaya, *Kinet. Katal.*, **7**, 1074 (1966); (b) R. Szentrimay, P. Yeh, and T. Kuwana, *ACS Symp. Ser.*, No. 38 (1977).
(20) J. D. Johnson, Ph.D. Thesis, University of North Carolina, Chapel Hill, N.C., 1962.
(21) A. Merz and A. J. Bard, *J. Am. Chem. Soc.*, **100**, 3222 (1978).
(22) E. Laviron, *J. Electroanal. Chem.*, **52**, 395 (1974).
(23) D. F. Smith, University of North Carolina, unpublished results.
(24) Due at least in part to shift in reference electrode junction potential.
(25) J. L. Crowley and H. Rapoport, *Acc. Chem. Res.*, **9**, 135 (1976).